Resistance to mold development assessment of bio-based building materials

M. Viel, F. Collet, Y. Lecieux, M.L.M. François, V. Colson, Christophe Lanos, A. Hussain, M. Lawrence

1 Resistance to mold development assessment of bio-based building

2 materials

3 Marie Viel[a, *], Florence Collet[a], Yann Lecieux[b], Marc François[b], Valentin Colson[a, c], Christophe Lanos[a],

4 Atif Hussain[d] and Mike Lawrence[d]

5 [a] *Université de Rennes, Laboratoire Génie Civil et Génie Mécanique, BP 90422, Rennes,*

6 *France*

7 [b] *Université de Nantes, Institut de Recherche en Génie Civil et Mécanique, BP 92208, Nantes,*

8 *France*

9 [c] *CAVAC Biomatériaux, Le Fief Chapitre, Sainte Gemme la Plaine, France*

10 [d] *BRE Centre for Innovative Construction Materials, Department of Architecture and Civil Engineering,*

11 *University of Bath, BA2 7AY, United Kingdom*

12 * Corresponding author: marie.viel@univ-rennes1.fr

13

14 Abstract

15 Nowadays, insulating building materials are developed from the valorization of agro-resources. They

16 show high ecological and hygrothermal performance. Before making them available on the market,

17 there is a need to classify them according to their decay resistance. This paper aims to propose a test

18 method that qualifies bio-based composites with respect to their performance. An accelerated aging

19 test was carried out on 5 composites made with two different agro-resources (hemp and rape) and

20 with different binders. It consists of exposing the specimens to (30 °C; 90% RH) for three months.

21 During the test, the specimens are regularly weighed and photographed. The sample mass and the

22 percentage of surface contaminated by fungi are measured along the test. Finally, a microscopic view

23 allows identifying the species of the developed molds.

24

25 Keywords

28

1. Introduction

The development of new insulating building materials from agro-resources of local agriculture (hemp shiv, flax shiv, wheat straw, etc.) is currently booming. The main quality of these materials is their hygrothermal performance when compared with traditional building materials. However, before they can be made available in the market, others characteristics need to be evaluated such as mechanical performance and durability. This paper investigates the decay resistance of the newly developed composites. Bio-based materials are assumed to be highly sensitive to the mold growth due to their chemical composition: cellulose, hemicellulose, lignin and proteins.

The molds are produced by wide variety of microorganisms, mainly microscopic fungi and yeasts. These play an important role in the decomposition of plant materials. These microorganisms grow and reproduce very quickly, spreading spores and mycelium.

These microorganisms may already be present inside building materials (walls, partitions, ceilings) or may be directly introduced into homes through ventilation. Their growth depends on various factors, in particular: flood, water leaks (roof or pipework), poorly-ventilated spaces (in kitchen, in bathroom)and building seals [1,2]. In all cases, the fungi will grow when materials contain free water. For wood, the water content at the fiber saturation point ranges from 20 to 30 %. The appearance of fungi induces a mass loss of between 5 and 10 % and the mechanical properties decrease between 20 and 80 % depending on the type of material [3]. The molds collect water, nutritional substances and minerals needed for their synthesis from the surrounding environment and the materials [2,4–7].

Although fungi are present in the atmosphere, higher concentrations may result in adverse health effects. Indeed, many fungal components are likely to cause adverse effects on the health of exposed individuals. Mycelial fragments can be present in ambient air and could be inhaled. Their walls contain glucans (complex sugar) with inflammatory properties. Spores may also cause allergic reactions such as allergic rhinitis or worsening of asthma symptoms. Furthermore, fungi release toxins of which toxicity may persist after the fungi have ceased to grow. The threshold of sensitivity varies from one individual to another, and according to the type of mold for each person. The individual response and the experienced symptoms vary considerably depending on the individual sensitivity and the duration of exposure to the fungi. Infants, children, the elderly, pregnant women and people suffering from

59 respiratory diseases, allergies, asthma and weakened immune systems are usually more sensitive to

60 mold exposure. Likewise, the severity is not necessarily proportional to the extent of exposure. Mold

61 prevention and remediation in new and existing housing is thus not solely an aesthetic issue, but also

62 one of public health and hygiene [1,5,8,9].

63

64 There is therefore a need to classify materials depending on their decay resistance in order to use

65 them appropriately. To qualify the durability of materials, different methods and standards exist such

66 as: Johansson method [10], AWPA Standard E24-06 [11], ASTM 2012 [12] or BSI EN ISO 846 – 1997

67 [13], assessing the resistance of specimen surface to mold growth after fungi inoculation. For each of

68 these methods, the intensity of specimen's mold growth is visually rated using a scale during the test

69 period. Thus, this is a somewhat subjective type of assessment.

70

71 The aim of this paper is to develop a method to qualify bio-based composites with respect to their

72 resistance to mold development. The composites were exposed over a three months period to

73 unfavorable conditions: 30°C and 90% RH. These conditions are expected to initiate and accelerate

74 mold growth on the surface of bio-based panels. The composite specimens were made with two

75 different agro-resources (hemp and rape) mixed with different binders. They are tested without prior

76 sterilization or inoculation with mold. Specimens are regularly weighed and photographed during the

77 test. The evolution of two indicators is thus measured over time: the sample mass and the percentage

78 of its surface contaminated by fungi. Two ways are used to rate the contaminated area: visual

79 inspection as stated previously and digital image correlation (DIC). The latter method is developed in

80 this work for quick quantification of the contaminated surface of the specimens by molds in an

81 objective manner unlike the visual evaluation. At the end of the test, microscopic views are analyzed in

82 order to identify the mold species which have contaminated the composite.

83

84 **2. Materials and methods**

85 **2.1. Bio-aggregates**

86 Two types of aggregates are considered in this study: hemp shiv and rape straw (Fig. 3). The main

87 characteristics of these aggregates are reported in Table 1. The particle size distribution, bulk density

88 and thermal conductivity were obtained using protocols set by RILEM TC 236-BBM [14]. The moisture

89 buffer value (MBV) is measured for bulk materials according to a method based on the NORDTEST

90 protocol [15].

91

92 The hemp shiv is a commercial product (Biofibat – CAVAC, France) commonly used to produce hemp

93 concrete. The mean width of particles (W50) is 2.2 mm and the mean length (L50) is 8.0 mm. The

94 maximal width is 5.0 mm and the maximal length is 19.0 mm. The thermal conductivity is 64.1

95 mW/(m.K) for bulk density around of 110 kg/m^3. The MBV is 2.35 g/(m².%RH). According the

96 classification of the Nordtest project, bulk hemp shiv appears as an excellent hygric regulator (MBV

97 higher than 2 g/(m².%RH)).

98

99 The rape straw (supplied by CAVAC, France) is the residual portion of the threshing of rape commonly

100 used for animal bedding, mulching or animal feeding. The mean width of particles is 3.1 mm and the

101 mean length is 15.9 mm. The maximal width is 8.5 mm and the maximal length is 45.2 mm. The

102 thermal conductivity is 49.9 mW/(m.K) for bulk density around of 75 kg/m^3. The MBV is 2.25

103 g/(m².%RH). According the classification of the Nordtest project, it is an excellent hygric regulator

104 (MBV higher than 2 g/(m².%RH)).

105

106 *Table 1 : Main characteristics of hemp shiv and rape straw*

Aggregates	Hemp shiv	Rape straw
Mean Width (W50, mm)	2.2	3.1
Maximal width (mm)	5.0	8.5
Mean Length (L50, mm)	8.0	15.9
Maximal length (mm)	19.0	45.2
Bulk density (kg/m^3)	107.9	73.3
Thermal conductivity (mW/(m.K))	64.1	49.9
MBV (g/(m².%RH))	2.35	2.25

107

2.2. Composite formulations

109 The composite formulations are developed within ISOBIO project [16]. During this project, several

110 lines of research are studied with the aim of producing, from these bio-aggregates and a green binder,

111 a rigid insulation panel. The main lines of research are as follows:

112 ▪ Use the adhesive properties of aggregates after treatment,

113 ▪ Use crosslink binders to improve the mechanical properties and water repellence of

114 composites,

115   ▪   Use a sol-gel treatment to improve the water repellence of composites.

116

117   Numerous formulations were investigated and the five best ones are selected to produce specimens

118   for this study. They are made of rape straw or hemp shiv, treated or not, mixed with or without binders

119   and with or without additives. The formulations are summarized in Table 2.

120

121   C1 composites are made of rape straw after exposure to alkali treatment. Preliminary work showed

122   that after alkaline and thermal treatments on rape straw, the produced composites have good

123   cohesion, which is induced by the polymerization of soluble components. This formulation has an

124   advantage to only use treated rape straw and thus 100 % bio-based insulation panels can be

125   produced in the same line as the hemp-straw composites [17].

126

127   C2 composites are made of hemp shiv mixed with a binder formulated using a starch derivative and a

128   crosslinker. The starch and its derivatives have good adhesive properties on the lignocellulosic

129   substrates. However an important issue is the low energy chemical bonds (Van der Waals and

130   hydrogen bonds), which ensure starch cohesion. Moreover, they can be easily hydrolyzed by water,

131   resulting in poor water resistance of the composite. Therefore a crosslinker is added to create, after a

132   thermal activation, covalent bonds between the starch macromolecules chains and thus, to form a

133   three-dimensional network in order to improve the mechanical strength and the water resistance of the

134   composite. C3 composites are made using the same formulation as C2 composites, but 2 % of

135   paraffin is added, to improve its water repellence.

136

137   C4 composites are made of hemp shiv coated with a sol-gel treatment to improve their water

138   repellence. For the preparation of the sol-gel, 1 M of TEOS was added to a mixture of 4 M distilled

139   water, 4 M of absolute ethanol and 0.005 M of nitric acid. 0.015 M of HDTMS was added to the above

140   mixture as the hydrophobic agent. The sol was vigorously stirred at 40 °C and atmospheric pressure

141   for nearly 2 hours. The sols were allowed to age for 96 hours in closed container at room temperature

142   before to be mixed with the hemp shiv in order to coat them. In the case of C4 composites, this sol-gel

143   coating also serves as a binder. C5 composites are made of the same coated aggregates as C4

144   composites and the same binder as C2 composites. Compared to C4 composites, the addition of the

145   binder improves the mechanical properties.

146

147   *Table 2 : Specimens composition*

Formulations	C1	C2	C3	C4	C5
Aggregates	Rape straw 100 %	Hemp shiv 90 %	Hemp shiv 88 %	Hemp shiv 100 %	Hemp shiv 90 %
Treatment	Alkali	Without	Without	Sol-gel	Sol-gel
Binder	Without	8% Starch derivative 2 % Crosslinker	8% Starch derivative 2 % Crosslinker	Without	8 % Starch derivative 2 % Crosslinker
Additive	Without	Without	Paraffin 2%	Without	Without
Solvent	Without	Water 33 % of dry content	Water 33 % of dry content	Without	Water 33 % of dry content

148

2.3.   Composite production process

150   For preparation of C1, C2, C3 and C5 composites, the bio-aggregates (treated, coated or not) are

151   moistened with the solvent and/or the binder, if any. Three specimens are produced from the same

152   mixture. This batch is divided into three equal parts (A, B and C) and each part is introduced in one of

153   the three cells of a mold. Each part is compacted 5 times at 0.25 MPa in the mold and then placed in

154   an oven at 190 °C for 2 hours. The three specimens of dimensions 100 x 100 x 50 mm^3 are demolded

155   once they cool down to room temperature (Figure 1).

157   *Figure 1 : Flow-chart of composites production (except C4 formulation)*

158
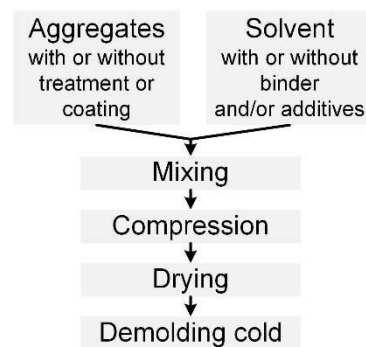
159   For C4 formulation, mixing of the constituent materials, hemp shiv (75 vol%) and sol (25 vol%), were

160   carried out manually to achieve a uniform mixture. The mass of the materials was pre-calculated to

161   target a final density of 175 kg/m^3 for the composites. Hemp shiv were mixed with the sol and then

162   placed into a phenolic ply mold, tamped down and left for overnight in the oven at 80 °C. The

163 specimens of dimensions 100 x 100 x 50 mm^3 were removed from the molds and transferred to a

164 conditioning room at 19 °C and 50% RH.

165

166 Figure 2 shows the produced composites and Table 3 gives their apparent density. The composites

167 based on hemp shiv have very close densities ranging from 173 to 203 kg/m^3. The composite based

168 on rape straw (C1) has the highest density (288 kg/m^3) due to much higher density of the aggregate

169 after alkali-treatment which reduces intra and inter-particle porosity. The C1 composites have the

170 highest pH (10) due to alkali treatment. The composites made with starch derivative based binder and

171 crosslinker (C2, C3 and C5), have an acid pH of 6. The composites which are glued with sol-gel (C4),

172 have the lowest pH (4).

173

175 *Figure 2 : Developed composites*

176

177 *Table 3 : Apparent density and pH surface of composites*

N°	C1	C2	C3	C4	C5
Density (kg/m^3)	287.66 ± 9.49	181.02 ± 2.82	184.21 ± 1.51	173.92 ± 6.11	203.10 ± 4.20
CoV	3.30 %	1.56 %	0.82 %	3.51 %	2.07 %
pH	10	6	6	4	6

178
179

2.4. Methods for characterization

2.4.1. Biological aging

182 The accelerated aging test evaluates the fungal resistance of the composites at given temperature

183 and humidity and is schematized in Figure 3. After stabilization at 23°C and 50% RH, the biological

184 aging tests are performed in a climate chamber (Vötsch VC0034, Figure 3.1) under controlled

185 temperature and relative humidity at 30°C and 90% RH for three months. The specimens are tested

186 without prior sterilization or inoculation with mold to closely reproduce a real exposure situation.

187

188 For each formulation, three specimens are tested. Each specimen (3 specimens per formulation) is

189 placed in a plastic box to prevent contamination between specimens. In order to facilitate image

190 treatment, the specimen is prevented from moving in the box, by making use of the aluminum

191 adhesive block. Furthermore, the experimental bench allows to take pictures of the top surface of the

192 specimens in a consistent manner (Figure 3.3). Every week day, the specimens are weighed (Figure

193 3.2) and visually inspected. Pictures are captured with a camera (Coolpix 8700, 8 Megapixels, Nikon).

194

195 For the analysis, mass variation from the steady state point is related to the exchange surface area

196 (including horizontal top and lateral surfaces of the specimen). The mass loss of each formulation is

197 expressed as the mass ratio between the maximal mass and this of the given time, using Equation (1).

198 $$ML = \frac{m_{max} - m}{m_{max}} \; x \; 100 \hspace{4cm} (1)$$

199 Where ML is the mass loss (%); m_{max} is the maximal mass of composite (g) and m is the mass of

200 composite at the given time (g).

201

202 On the final day of the test, the samples are visually evaluated for mold growth according the rating

203 scale of BSI EN ISO 846 – 1997 [13], which is shown in Table 4. This method is subjective. Thus, the

204 final rating is the average value of the given rating by each author in this publication, making a total of

205 8 people.

206

207 *Table 4: Assessment of growth following the BSI EN ISO 846 – 1997 [13]*

Intensity of growth	Evaluation
0	No growth apparent under the microscope.
1	No growth visible to the naked eye, but clearly visible under the microscope.
2	Growth visible to the naked eye, covering up to 25 % of the test surface.
3	Growth visible to the naked eye, covering up to 50 % of the test surface.
4	Considerable growth, covering more than 50 % of the test surface.
5	Heavy growth, covering more than 75 % of the test surface.

208

209 The chosen method has an advantage of being non-intrusive unlike other methods found in the

210 literature:

211   •   Use of adhesive to remove fungal spores from the substrate and then scanning of mold

212   imprint [18];

213   •   Scanning two sides of the specimen [19].

214 It should be noted that during the entire period of the test the biotope remains undisturbed.
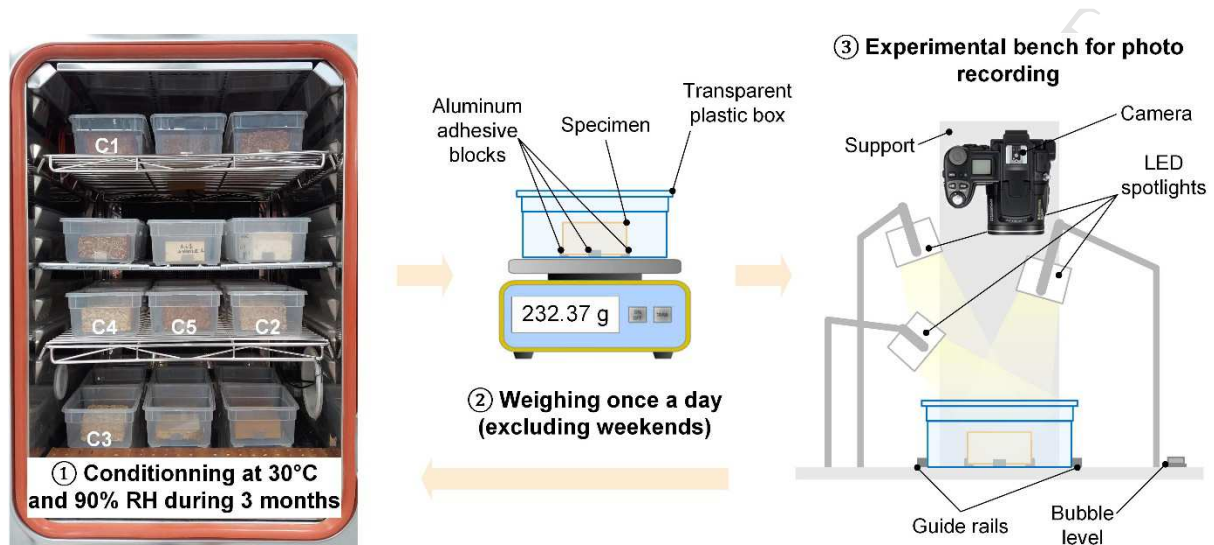
215

216

217 *Figure 3: Experimental device for biological aging: conditioning, weighing and photo recording*

218

2.4.2. *Image analysis*

220 In this study, the chosen contamination indicator is the relative photographed surface contaminated by

221 mold with reference to the total surface. A similar approach is used by various researchers in the field

222 such as Nielsen et al [2], Johansson et al [10], Clausen and Yang [18] and Garzon-Barrero et al [19].

223 To evaluate the mold growth between two dates t_0 and t, two photographs of the same specimen

224 have been taken. In this study, a very simple experimental device has been chosen (Figure 3,

225 Experimental bench for photo recording) to avoid use of sophisticated equipment. However for image

226 analysis, it is necessary to use or to develop specific IT-tools.

227

228 The image analysis is performed in two steps:

229   •   Firstly, the displacement field between images recorded at t_0 and t is computed. This

230   displacement may be due to operator handling (such as accidental motion of the specimen or

231   the camera) or caused by a dilatation of the composite due to swelling induced by moisture

232   change. This step is achieved, thanks to Digital Image Correlation (DIC) analysis, using the

233   code DIGIMCO developed by Marc François in MATLAB software and freely available. Similar

9

234   tools, whether free or commercial software exist [20,21] and have been used for several years

235   to perform displacement field measurement, or to evaluate mechanical properties [22–24].

236   • Secondly, the location of mold is revealed thanks to the error map of correlation between

237   images recorded at time t_0 and t. It represents the discrepancy between the two images once

238   correlated in space. A gray level difference reveals the presence of molds.

239

240   A digital image is a set of data produced by recording variation in the intensity of a signal. It's a matrix

241   of r rows and c columns. Each pixel has a value that represents the brightness of a given color at any

242   specific location. In this paper, the image f and the image g designate the images of an object

243   recorded in the initial state (at time t_0) and in the final state (at time t) respectively. The discrete

244   functions $f(X)$ and $g(X)$ denote the gray levels associated with pixel of the image f and g respectively,

245   located at position X (the coordinates are in pixels). The location of a given texture point is referred to

246   be as X in image f and x in image g (see Figure 4). Possible transformations between two images are

247   schematized in Figure 4 (i.e. dilatation, translation and rotation). The first step of the analysis is to

248   compute the displacement field $\mathbf{u}(X)$ which gives the best fit between images f and g. The texture of

249   the two images is quite similar and is used to determine this fit.
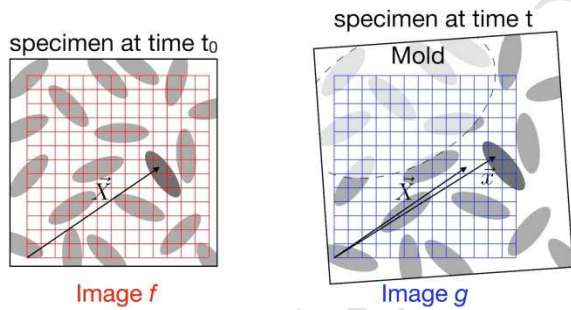
250

251   *Figure 4: Digital image correlation between initial image f (time t_0) and current image g (time t)*

252   The displacement $\mathbf{u}$ is defined by:

253    $\mathbf{x} = \mathbf{X} + \mathbf{u}$ (2)

254   Supposing a homogeneous deformation, the mapping of the transformation is a parameterized field of

255   the form:

256    $\mathbf{x} = \mathbf{F}.(\mathbf{X} + \mathbf{T})$ (3)

257   where T is a translation vector described by the parameters λ_1 and λ_2.

258    $\lambda_1 = T_1$ (4)

259    $\lambda_2 = T_2$ (5)

260 and F is the deformation gradient tensor described by the parameters $(\lambda_3, \lambda_4, \lambda_5, \lambda_6)$:

261 $\lambda_3 = n\,(F_{11} - 1)$ (6)

262 $\lambda_4 = n\,(F_{12})$ (7)

263 $\lambda_5 = n\,(F_{21})$ (8)

264 $\lambda_6 = n\,(F_{22} - 1)$ (9)

265 where n is a weighting factor. It must be emphasized that the tensor **F** includes pure deformation, rigid

266 rotation and dilatation. The DIC method [22] is based on an assumption of optical flow conservation

267 between images f and g whose texture does not significantly differ thus $f(X) = g(x) = g(X + u)$ (with

268 a possible error). The experimental conditions are compatible with these assumptions since the

269 brightness of the images and the color of the composites do not significantly evolve during the test. To

270 find the displacement u or the parameters λ_i, the sum of squared differences φ of the gray levels have

271 to be minimized over the zone of interest $-Z_i-$ which corresponds in this study to the whole

272 photographed face of the composite is:

273 $\varphi(\lambda_1, \lambda_2, \lambda_3, \lambda_4, \lambda_5, \lambda_6) = \sum_{X \in Z_i} \big(g(x) - f(X)\big)^2$ (10)

274 However the computation of the displacement field u is not the objective of this study. It is only

275 necessary to compare images f (original) and g (with mold), pixel to pixel, at exactly the same location.

276 Here, the presence of mold changes the gray level. The zones affected by mold are supposed to be

277 large with respect to the texture size of the image of the composite. Then, assuming a uniform

278 variation of the gray level b, (due to the presence of mold) the equation 10 becomes:

279 $\varphi(\lambda_1, \lambda_2, \lambda_3, \lambda_4, \lambda_5, \lambda_6) = \sum_{X \in Z_i} \big(g(x) + b - f(X)\big)^2$ (11)

280 The result of the minimization (i.e. the computation of parameters λ_i or the displacement field u) is not

281 modified by the presence of b since it does not modify the gradient of φ [22]. Figure 5 illustrates the

282 method. The function $f(X)$ represents a 1D example of gray level in the initial image f (without mold).

283 The function $g(X)$ represents the final grey level of image g in which molds have changed the gray

284 level of some domains. A rigid body motion is visible. Once computed the best correlation (Equation

285 11) the maximum and minimum shall match between $f(X)$ and $g(x)$. Then, the difference $g(x) - f(X)$

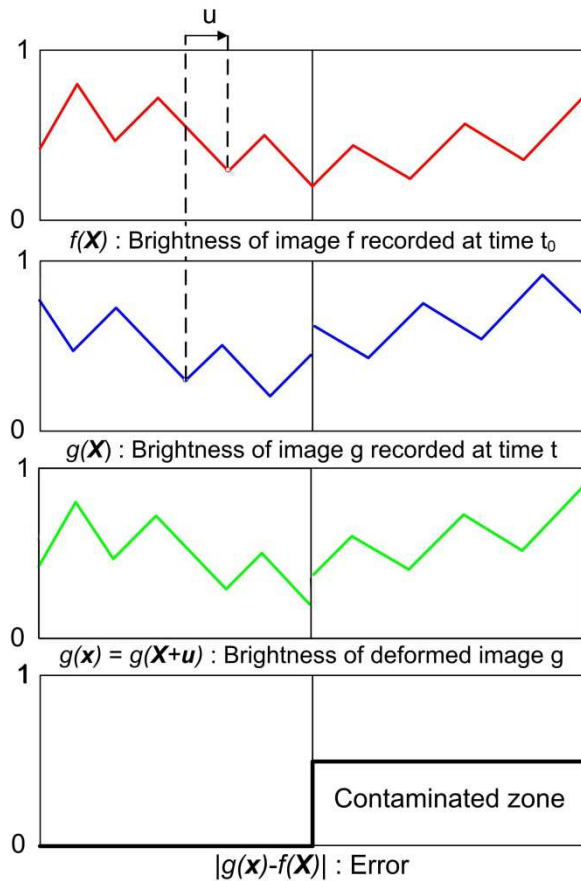286 exhibits the location of the colonization.

287

11

288

289 *Figure 5: Relative brightness, of image g and f: an error involves the detection of a new object.*

290

291 As an example, a test was performed on an 8-bit image (brightness coded from 0 to 256) of the

292 composite (C1) without visible mold (see Figure 6). The reference image 6.a is compared with the

293 image (6.b). It is a photography of the same composite taken 24 hours later also free of molds. In

294 image 6.c an inscription is added with drawing software. Then, with DIGIMCO, the uniform

295 displacement field which allows to superimpose the images 6.a and 6.b first, and then the images 6.a

296 and 6.c are searched. Once the displacement field has been obtained, the map of the correlation

297 errors between 6.a and 6.b is displayed on the image 6.d. On the image 6.e the map of the correlation

298 errors between 6.a and 6.c is also displayed. On the error map 6.e, the inscription added to the image

299 6.c is clearly visible while the error map 6.d is uniform and has virtually zero errors. From this error

300 map, a thresholding operation (binarization) makes it possible to isolate the change, in this example,
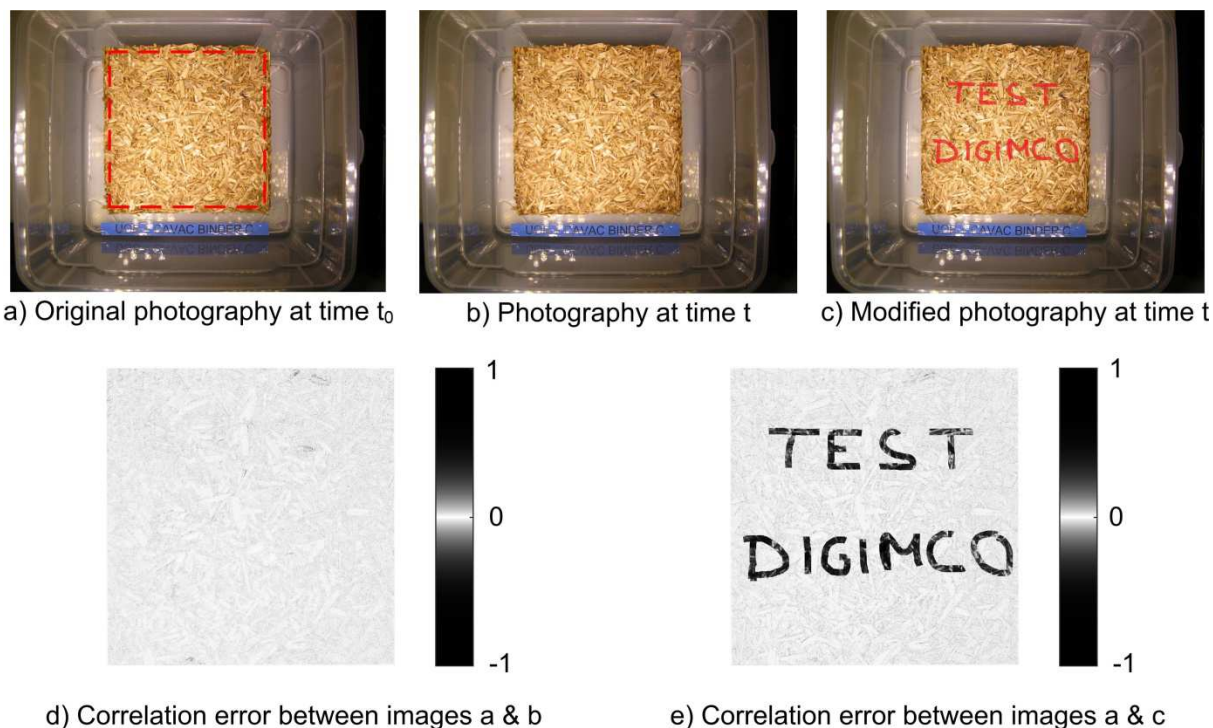
301 the inscription "Test DIGIMCO".

302

a) Original photography at time t_0 b) Photography at time t   c) Modified photography at time t

d) Correlation error between images a & b   e) Correlation error between images a & c

303

304   *Figure 6: Example of object detection using DIC*

305

306   It should be emphasized that in the traditional use of the DIC method, the surface of the studied object

307   is covered with a randomly painted speckle pattern. This surface preparation allows to obtain a highly

308   contrasted and unstructured image. This is not the case for this test. The surface of the composite acts

309   as the randomly speckle pattern. The presence of hundreds of particles entangled without a regular

310   pattern on the visible surface of the composite makes it possible to apply the DIC method without

311   modifications. Thus, using the DIC does not require any treatment or modification of the environment
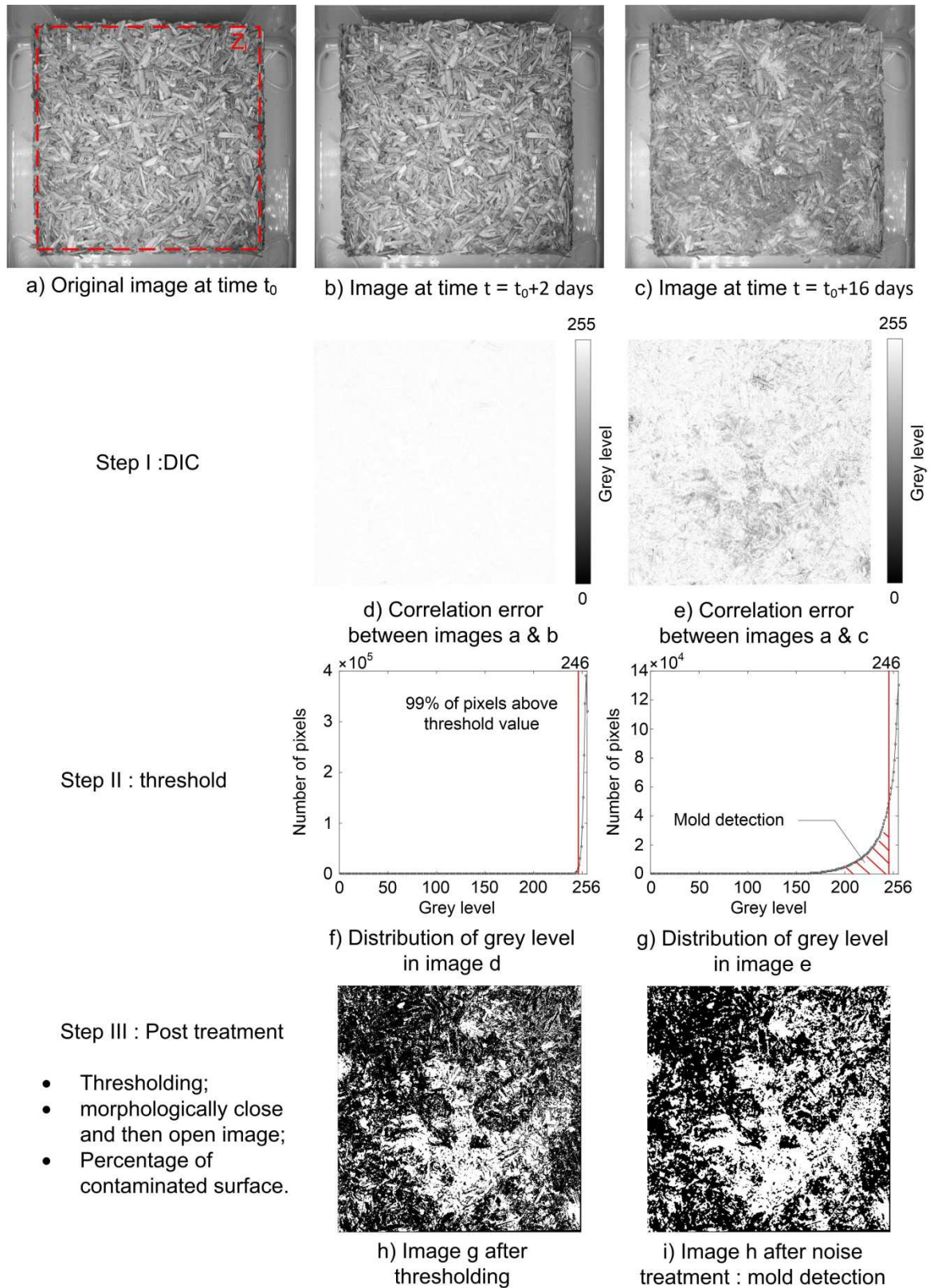
312   likely to modify the growth of the studied organism.

313

a) Original image at time t_0

b) Image at time $t = t_0+2$ days

c) Image at time $t = t_0+16$ days

Step I :DIC

d) Correlation error between images a & b

e) Correlation error between images a & c

Step II : threshold

99% of pixels above threshold value

Mold detection

f) Distribution of grey level in image d

g) Distribution of grey level in image e

Step III : Post treatment

- Thresholding;
- morphologically close and then open image;
- Percentage of contaminated surface.

h) Image g after thresholding

i) Image h after noise treatment : mold detection

314

315   *Figure 7: Procedure of image analysis, DIC and post-treatment applied on composite C5*

316

317   Once correlation error maps are calculated for each image, the post-processing operation is

318   performed with MATLAB. The entire image processing procedure is summarized in Figure 7. It

319 requires at least 3 pictures: the initial image of the composite 7.a, an image without apparent molds b)

320 and the image to be analyzed 7.c. After obtaining correlation maps 7.d and 7.e, a thresholding is

321 performed. The choice of the threshold value is by definition arbitrary. However, the study of the

322 correlation errors map obtained for an image supposed without fungi (see a sample at $t = t_0 + 2$ days

323 on Figure 7.d) allows to propose a coherent and systematic threshold value. On this example, 99 % of

324 the pixels have a gray level greater than 246 (see Figure 7.f). This value was used for the thresholding

325 operations performed on the photographs taken the following days.

326

327 Pixels which value is below this threshold value are considered to be contaminated (see Figure 7.g).

328 After the thresholding, the Figure 7.h is obtained). A morphological operation of opening and closing of

329 the black-and-white image is then performed to filter the isolated pixels (with the "imopen" and

330 "imclose" function of MATLAB) and reduce apparent measurement noise. Finally, the number of white

331 pixels and black pixels in the image are counted to get the percentage of surface contaminated by

332 fungi.

333

334 ### *2.4.3. Microscope visualizations*

335 After the three-month test period, microscope visualizations are performed in this study to identify the

336 type of mold which are developed on the contaminated composite surface. The infected shiv are

337 collected with a pair of tweezers and are observed under a microscope LCD (5 Megapixels, Bresser).

338 Pictures are captured at 50x and 125x magnification. Then, the pictures are opened with Image J

339 (NIH) with the addition of the Microscope Measurement Tools plugin (Fiji) to take measures and scale

340 bar is added. The microscope is calibrated for a 50x and a 125x magnification using an optical fiber to

341 125 ± 0.7 µm in diameter (Corning® SMF-28® Ultra Optical Fiber). The determined scale is the

342 average value of five measurements and is validated using a coated optical fiber to 242 ± 5.0 µm in

343 diameter (Corning® SMF-28® Ultra Optical Fiber).

344

345 ## 3. Results and Discussions

346 ### 3.1.   Macroscopic visualizations

347 Figure 8 gives the pictures of the C1 to C5 specimens at several times during the test period. The

348 visual inspection shows that during this test, C1 composite does not show any fungal development.

349   The other composites show gradual growth of molds, more or less, quickly. C2 and C3 composites do

350   not have their surface strongly affected unlike the C4 and C5 composites. C5 composite has the most

351   affected surface. First fungi mainly appear between the shiv on C2, C3, C4 and C5 composites

352   between the fourth and the seventh day. The multiple colors of molds (grey, white and yellow) would

353   suggest at least two types of fungi have contaminated the composite surfaces.
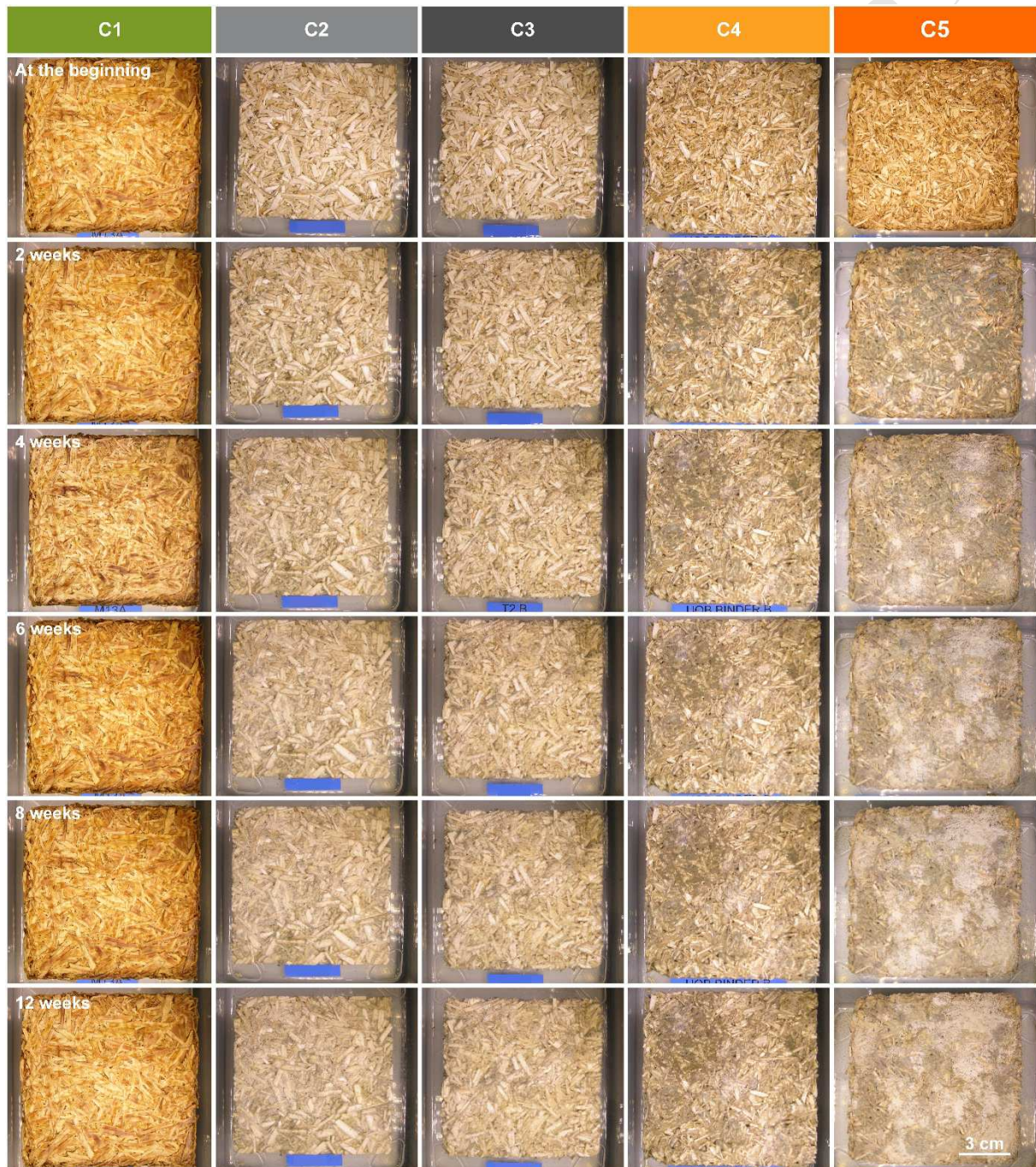
354

356   *Figure 8: Specimens on the weeks 0, 2, 4, 6, 8 and 12 of ageing test*

357

358 Figure 9 gives the average ratings of the visual evaluation given by the authors with the rating scale of

359 BSI EN ISO 846 – 1997 [13] at the end of test. C1 composite does not have visible fungi. C3

360 composite has less than 25 % of its surface contaminated. C2 and C4 composites have between 25

361 and 50 % of their surface contaminated, with C4 being probably the more contaminated of the two.

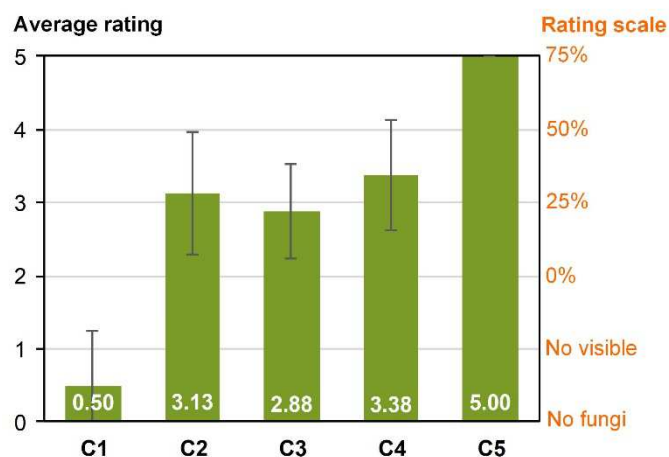362 Finally, C5 composite has more than 75 % of its surface contaminated.

363

364

365 *Figure 9: Average rating of mold growth on specimens with the rating scale of BSI EN ISO 846 – 1997 (British*
366 *Standards Institute, 1997) after 12 weeks at 30°C and 90% RH*

367

368 **3.2. Mass loss**

369 Figure 10 gives the mass variation at 30°C and 90% RH from the steady state point (23°C and 50%

370 RH), related to the exchange surface area (including top and lateral surfaces of specimens). During

371 the first week of exposure, all specimens show an increase in mass due to water vapor adsorption

372 resulting in a water content of about 20 % in specimens. From the eighth day, C5 composite slightly

373 decreases in mass. From the ninth day, C2, C3 and C4 composites slightly decrease in mass too. The

374 mass loss is due to the fungi development. C5 composite has the highest mass loss and C3

375 composites has the lowest mass loss. The two others composites have similar mass loss.in contrast,

376 from the eighteenth day, C1 formulation slowly increases in mass before stabilizing and reaching
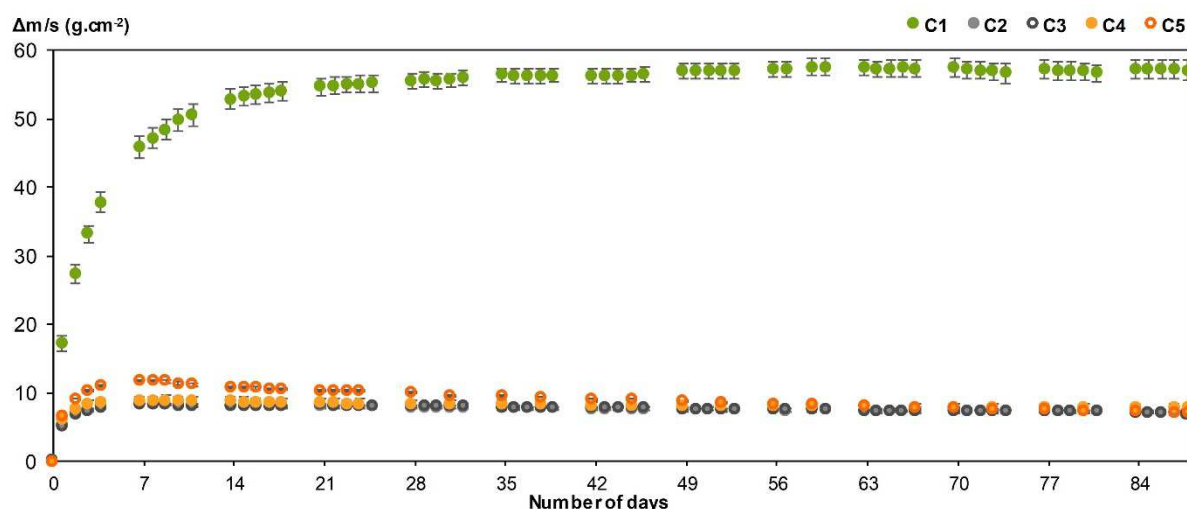
377 water content of about 54 % at the end of the test.

378

379

380
381

382

383 Figure 11 and Table 5 give the mass loss for C2, C3, C4 and C5 composites during the test. The

384 kinetics of mass loss increase linearly for the four formulations after the first week. This week certainly

385 corresponds to the time needed to reach a water content threshold in the specimens in order to trigger

386 mold growth. The correlation coefficients of the fitting curves are good as they are higher than 0.93.

387 C5 composite has the highest mass loss. C3 composite has the lowest mass loss. This is probably

388 due to the addition of paraffin which increases the water repellence. Moreover, the amount of

389 adsorbed water by the C3 composite is lower than other composites. C2 and C4 composites have

390 almost similar mass loss, thus the sol-gel coating does not have an impact on the kinetics of water

391 vapor absorption. At the end of the test, these three formulations have a mass loss about 1.15 %

392 whereas the C5 composite has the highest mass loss (4.28 %).
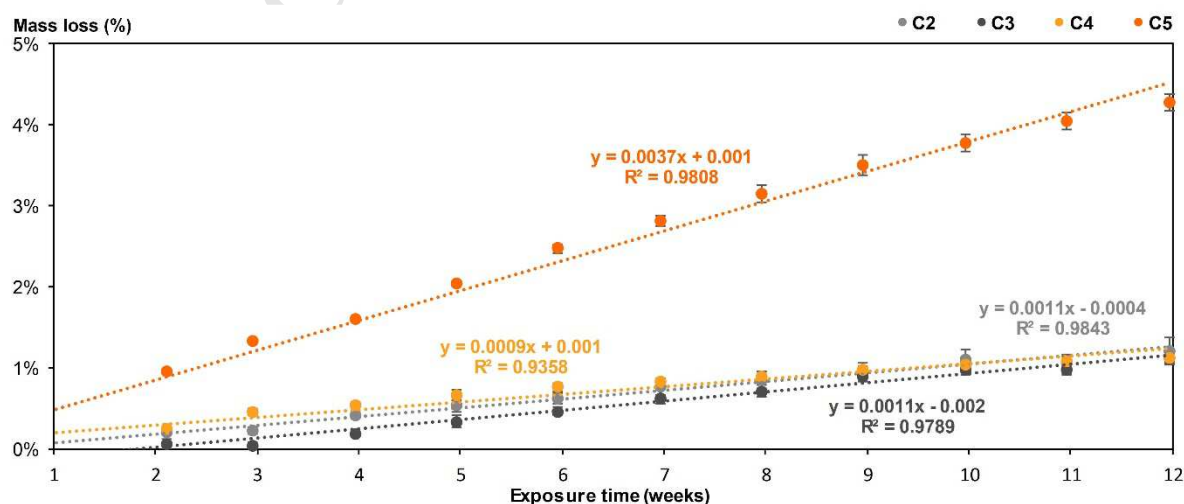
393

394

18

Figure 11: Mass loss for the tested composites during the ageing test

Table 5: Mass loss (ML, %) for the tested composites according to the exposure time (weeks)

Time (weeks)	ML C2	ML C3	ML C4	ML C5
0.96	0.00 ± 0.00%	0.00 ± 0.00%	0.00 ± 0.00%	0.00 ± 0.00%
2.11	0.21 ± 0.02%	0.06 ± 0.06%	0.23 ± 0.02%	0.94 ± 0.01%
2.96	0.23 ± 0.04%	0.03 ± 0.04%	0.45 ± 0.04%	1.33 ± 0.00%
3.96	0.42 ± 0.05%	0.19 ± 0.04%	0.53 ± 0.05%	1.61 ± 0.02%
4.96	0.53 ± 0.07%	0.33 ± 0.07%	0.66 ± 0.06%	2.03 ± 0.03%
5.96	0.62 ± 0.07%	0.46 ± 0.05%	0.76 ± 0.06%	2.47 ± 0.05%
6.96	0.76 ± 0.10%	0.62 ± 0.05%	0.82 ± 0.06%	2.81 ± 0.07%
7.96	0.85 ± 0.10%	0.71 ± 0.08%	0.89 ± 0.06%	3.15 ± 0.10%
8.96	0.95 ± 0.10%	0.90 ± 0.08%	0.97 ± 0.05%	3.50 ± 0.12%
9.96	1.10 ± 0.13%	0.97 ± 0.06%	1.04 ± 0.07%	3.78 ± 0.11%
10.96	1.05 ± 0.11%	0.98 ± 0.07%	1.08 ± 0.07%	4.04 ± 0.10%
11.96	1.21 ± 0.16%	1.13 ± 0.06%	1.12 ± 0.08%	4.28 ± 0.10%

3.3. Image analysis

Figure 12 shows some pictures taken at the end of the test which are used to get the percentage of surface contaminated by the fungi.
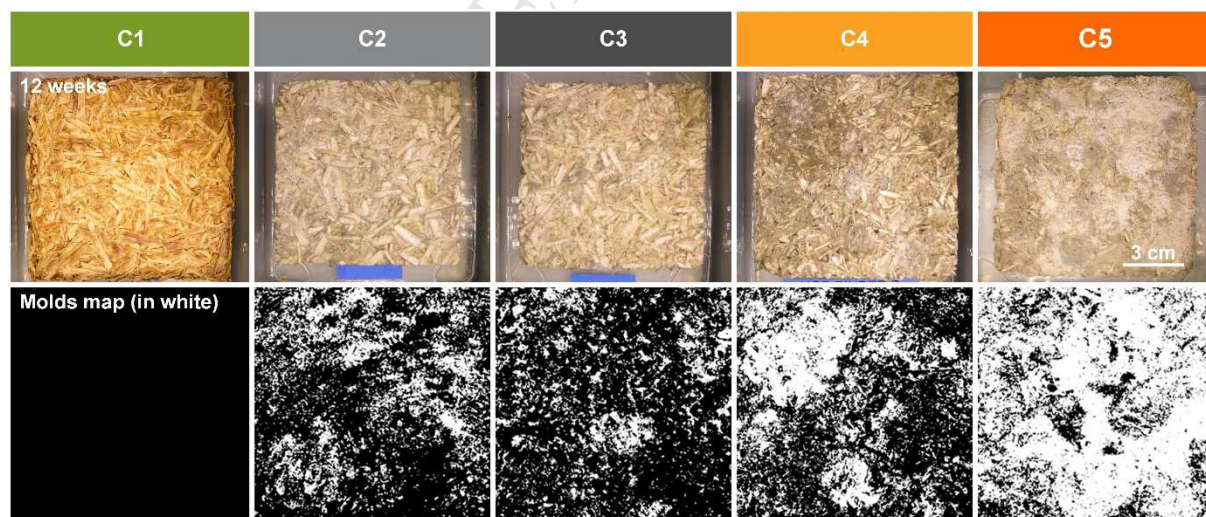

Figure 12 : Pictures before and after DIC treatment at the end of the test

The image analysis leads to the estimation of the surface ratio contaminated by the fungal growth during the test period at 30 °C and 90% RH (Figure 13). The different mold growth rate between

19

409   formulations are observed. Overall, C5 specimens have greater fungal growth with a higher standard

410   deviation between the three specimens. C3 specimens have the slowest rate of growth over the 12

411   week test period. For all specimens, there is a substantial increase in growth during the second week

412   which corresponds to the exponential phase of the fungal growth. During this period, the nutriments

413   are in excess. Thus, the first week corresponds to the time required by the growth conditions to

414   become favorable. The water content of specimens is around 10 % at the beginning of the test. 1

415   week is required to double this value. This phase is called the lag phase. During the third week, the

416   intensity of growth decreases. It corresponds to the slowdown phase. This is due to a depletion of the

417   culture medium (composites) and an accumulation of waste. This phase goes on two weeks in the

418   case of C5 composite. After the slowdown phase, the ratio of contaminated surface reaches a plateau

419   until the end of the test. This means that the growth becomes zero and therefore the molds that grow

420   multiply and replace those who die. This corresponds to the stationary maximum phase. At the end of

421   test, the mean contaminated surface is 21.87 % for C3 specimens, 28.36 % for C2 specimens, 34.69

422   % for C4 specimens and 77.50 % for C5 specimens. Growth kinetics observed here are consistent

423   with what is described in the biology literature [25]. These results suggest that the image analysis

424   method provides consistent and exploitable results for this study.
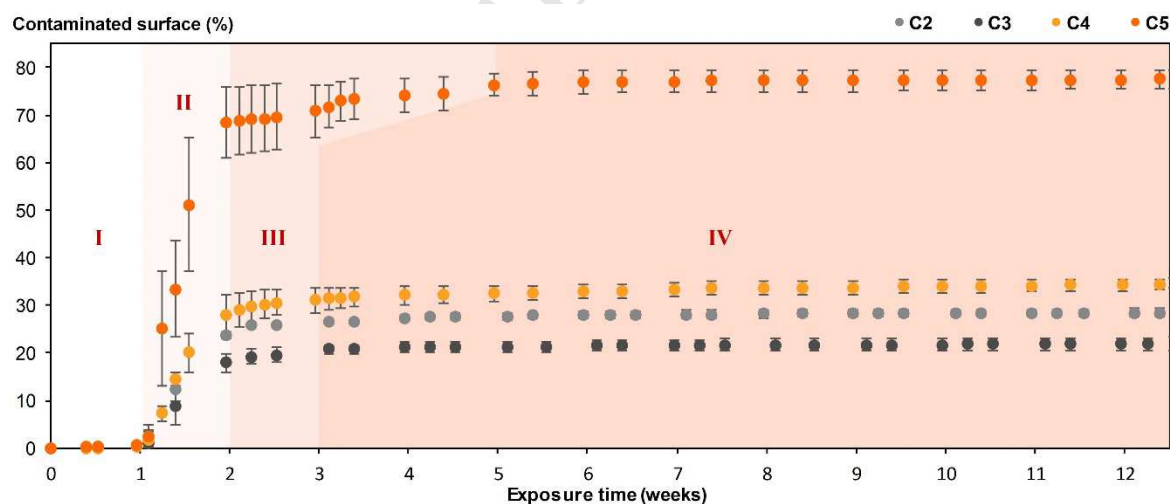
425

426

427   *Figure 13: Image analysis: rating of the contaminated surface of C2, C3, C4 and C5 composites exposed to 30℃*
428   *and 90% RH during the test period correlated to the fungal growth phases with I: Lag phase, II: Exponential*
429   *phase, III: Decelerating phase and IV: Stationary phase*

430

431   Table 6 compares the results obtained with the visual evaluation and the image analysis of the

432   contaminated surface of specimens at the end of the test. The average rating from visual evaluation

433   and from image analysis are close. However, the visual evaluation shows high discrepancy (up to 0.83

434   %) due to subjective effect. The image analysis leads to representative values as it is not subject to

435   subjective effect. It seems to be more accurate.

436

437   *Table 6: Average rating from visual evaluation compared to average rating from image analysis of mold growth on*
438   *specimens after 12 weeks at 30°C and 90% RH*

N°	C1	C2	C3	C4	C5
Visual evaluation	0.50 ± 0.76	3.13 ± 0.83	2.88 ± 0.64	3.38 ± 0.74	5.00 ± 0.00
Image analysis	0.00	3.13	2.93	3.43	5.00
Rating scale	No fungi	> 50 %	> 25 %	> 50 %	> 75 %

439

3.4.   Microscopic visualizations

441   After the test period, a sampling of mold is collected in order to identify the type of fungi, which is

442   responsible for the sample damage. Figure 14 shows some images of contaminated shiv taken using

443   the optical microscope at different magnifications. Table 7 summarizes the fungi characteristics which

444   have contaminated the specimens during the test. In the image 15.a, three species of mold are

445   present. The one which has a long stem with fluffy spherical white head is the *Aspergillus ruber* (AR).

446   It appears in more detail in the image 15.d. Under these white heads, a bright yellow spherical

447   cleistothecium is hardly discernible. It is *Eurotium rubrum* (ER), the sexual form of *Aspergillus ruber*

448   (AR) which is an asexual form. Still under these white heads, shiny smooth black globose pycnidia are

449   slightly visible, which belong certainly to the *Phoma sp.* genus and could be of the *Leptosphaeria*

450   *maculans* (LM) species. These two fungi appear in more detail in the image15.e. In images 15.b and

451   15.c, only one species is present. At the end of a long stem, there is a large white fan. It is the

452   *Penicillium brevicompactum* (PB). In the images of the specimens (Figure 8), the colored areas in

453   gray-brown correspond to this fungi. All contaminated composites (from C2 to C5) are infected by

454   these four species of mold.

455

456   The fungi are divided in three types of colonizers which need a minimum of available water for fungal

457   growth on the composites surfaces. The available water in the composites is defined by the water

458   activity (a_w) which corresponds to the equilibrium relative humidity (ERH) in percent in the materials.

459   Three colonizers are: primary ($a_w \leq 0.80$), secondary ($0.80 < a_w \leq 0.90$) and tertiary ($0.80 < a_w$) [26,27].

460   *Penicillium brevicompactum* (PB), *Eurotium rubrum* (ER) and *Aspergillus ruber* (AR) are primary

461 colonizers whereas *Leptosphaeria maculans* (LM) is secondary colonizer and may gradually become

462 the dominant fungi. This means that the fungi belonging to the primary colonizers have appeared as

463 soon as the water activity in the specimens made it possible. The secondary colonizers has appeared

464 later, certainly towards the end of the test as these colonizers needs higher water activity than the

465 primary colonizers [28,29]. However, they may create more damage than the primary colonizers

466 because they prefer more complex sugars as cellulose for example [30]. Continuous mass monitoring

467 could have been interesting in order to verify this hypothesis.

468

469 Finally, all these molds are potentially allergens. Indeed, these molds are associated with allergic

470 reactions such as allergic rhinitis or worsening of asthma symptoms. The threshold of sensitivity varies

471 from one individual to another, and according to the type of mold for the same person. The individual

472 response and the experienced symptoms vary considerably depending on the individual sensitivity

473 and the duration of exposure to the fungi. Moreover, all molds contain inflammatory substances that
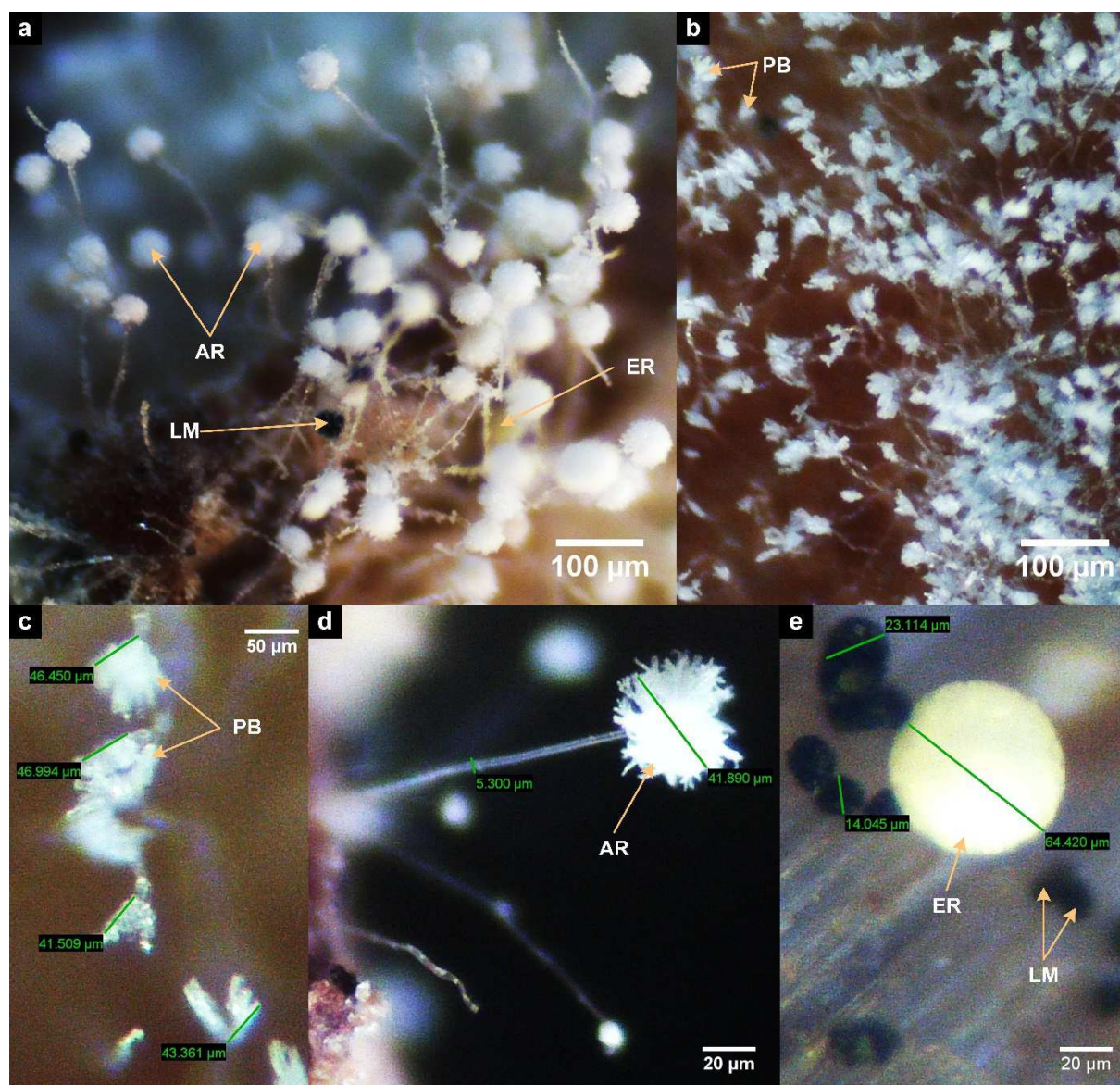
474 can produce inflammation to varying degrees.

475

476

477 *Figure 14: Optical microscope visualizations contaminated surfaces at the 50x (a, b and c) and 125x (d and e)*
478 *magnifications (AR: Aspergillus ruber, ER: Eurotium rubrum, LM: Leptosphaeria maculans and PB: Penicillium*
479 *brevicompactum)*

480

481 *Table 7: Fungi characteristics*

Species	*Penicillium brevicompactum*	*Eurotium rubrum* (sexual form)	*Aspergillus ruber* (asexual form)	*Leptosphaeria maculans* (anamorph Phoma lingam)
Genus	Penicillium sp.	Trichocomaceae	Aspergillus sp.	Phoma sp.
Order	Moniliale	Eurotiale	Moniliale	Sphaeropsidale
Class	Hyphomycetes	Eurotiomycetes	Hyphomycetes	Coelomycetes
Phylum	Deuteromycota	Ascomycota	Deuteromycota	Deuteromycota
Growth	Can grow between -2 and 30 °C with an optimum at 23 °C	Can grow between 5 and 37 °C with an optimum at 25 °C		Can grow between 15 and 32 °C with an optimum between 20 and 24 °C
Microscopic Appearance	Stipes smooth walled about 500 to 800 µm	Bright yellow spherical cleistothecium about	White radiate conidial heads	Shiny smooth black globose pycnidium

23

	in length. Broad terverticillate penicillin less than 40 µm long and 40 to 50 µm across the phialide tips.	60 to 150 µm in diameter	about 30 to 50 µm in diameter. Stalk smooth until 750 µm in length and 5 to 6.5 µm in diameter.	until 500 µm in diameter and developing under the epidermis and tearing at maturity.
Toxicity	Mycophenolic acid: Allergens	Quinonoid pigments: Allergens		Allergens
Scheme				
References	[31–33]	[31,34,35]		[36–38]

4. Conclusions

A protocol for evaluating the resistance to mold contamination of bio-based composites is proposed in this paper. It could be used to assess decay resistance of composites before making them available on the market. Accelerated aging test involves placing the composites in a favorable environment to mold growth for 3 months (30°C; 90% RH). Resistance to colonization of composites is then evaluated over time using three tests:

- Monitoring of external surface percentage contaminated by mold;
- Mass monitoring;
- Microscopic analysis.

The test protocol is easily reproducible since it requires commonly available equipment (a climate chamber, a camera and an optical microscope). The analysis protocol differs from existing intrusive fungal growth evaluation methods or based on subjective visual evaluations since it is fully automatized and do not needs any collecting of samples. The non-intrusive image analysis, based on the use of freely available IT-tools associated with mass monitoring allowed a rapid and quantitative assessment of mold growth and composite degradation.

24

498

499 Mass monitoring overlaps the effect of water absorption and decay. It provides information on long-

500 term degradation of composites. Moreover, it has been possible to determine the kinetics of apparent

501 mass loss. C1 composite does not show decay and the specimens increase in mass until they reach

502 equilibrium water content of about 54 % at the end of the test. For C2, C3, C4 and C5 composites, the

503 kinetics of mass loss increase linearly after the first week. This week certainly corresponds to the

504 needed time to obtain a sufficient water content in the specimens in order to trigger mold growth.

505

506 The percentage of the external surface contaminated by the composites is monitored by analyzing

507 images of the composites recorded during the test. The proposed method is based on an adaptation

508 of a DIC algorithm. Growth kinetics observed during the test is consistent with what is described in the

509 biology literature and suggests that the proposed method provides consistent and exploitable results.

510 The monitoring of the exterior surface contaminated by the composites allow a rapid and quantitative

511 evaluation of mold growth, essentially during the first 20 days.

512

513 The microscopic analysis make it possible to identify the species present on the composite. All

514 identified molds are potential allergens. These are mainly molds from primary colonizers. The

515 observation of a few individuals from secondary colonizers suggests that the degradation process of

516 the composites is still ongoing after 3 months of testing. Indeed, these colonizers would gradually

517 become the dominant fungi if nutrients are still available on the substrate. Moreover, they may create

518 more damage than the primary colonizers because they prefer more complex sugars. Continuous

519 mass monitoring could have been interesting in order to verify this hypothesis.

520

521 This test also makes it possible to establish a link between the chemical formulation of the composites

522 and their resistance to fungal colonization. The results suggest that the pH of given building material is

523 an important predictor of fungal susceptibility. Indeed, C1 formulation is the most resistant to fungal

524 development. This is due to having a surface pH of 10. The other formulations have a surface pH less

525 than or equal to 6 and have a more or less significant fungal development at the end of three months

526 of exposure test at 30°C and 90% RH. Another important predictor is the chemical composition of

527 specimens. However, C3 formulation contains paraffin to increase the water repellence. Thus, the

528 water content in the C3 specimens is lower than other specimens leading to lower kinetics of mold

529 growth on its exposed surface.

530

531 Acknowledgements

535

536 References

537 [1]   Nevalainen A, Seuri M. Of microbes and men. Indoor Air 2005;15:58–64. doi:10.1111/j.1600-
538   0668.2005.00344.x.
539 [2]   Nielsen KF, Holm G, Uttrup LP, Nielsen PA. Mould growth on building materials under low water
540   activities. Influence of humidity and temperature on fungal growth and secondary metabolism. Int
541   Biodeterior Biodegrad 2004;54:325–36. doi:10.1016/j.ibiod.2004.05.002.
542 [3]   Anagnost SE. Wood Decay, Fungi, Stain and Mold 2011.
543 [4]   Hoang CP, Kinney KA, Corsi RL, Szaniszlo PJ. Resistance of green building materials to fungal
544   growth. Int Biodeterior Biodegrad 2010;64:104–13. doi:10.1016/j.ibiod.2009.11.001.
545 [5]   Murtoniemi T, Hirvonen M-R, Nevalainen A, Suutari M. The relation between growth of four
546   microbes on six different plasterboards and biological activity of spores. Indoor Air 2003;13:65–
547   73. doi:10.1034/j.1600-0668.2003.01126.x.
548 [6]   Pasanen A-L, Rautiala S, Kasanen J-P, Raunio P, Rantamäki J, Kalliokoski P. The Relationship
549   between Measured Moisture Conditions and Fungal Concentrations in Water-Damaged Building
550   Materials. Indoor Air 2000;10:111–20. doi:10.1034/j.1600-0668.2000.010002111.x.
551 [7]   Yang VW, Clausen CA. Antifungal effect of essential oils on southern yellow pine. Int Biodeterior
552   Biodegrad 2007;59:302–6. doi:10.1016/j.ibiod.2006.09.004.
553 [8]   Ezeonu IM, Price DL, Simmons RB, Crow SA, Ahearn DG. Fungal production of volatiles during
554   growth on fiberglass. Appl Environ Microbiol 1994;60:4172–3.
555 [9]   Klamer M, Morsing E, Husemoen T. Fungal growth on different insulation materials exposed to
556   different   moisture   regimes.   Int   Biodeterior   Biodegrad   2004;54:277–82.
557   doi:10.1016/j.ibiod.2004.03.016.
558 [10] Johansson P, Ekstrand-Tobin A, Svensson T, Bok G. Laboratory study to determine the critical
559   moisture level for mould growth on building materials. Int Biodeterior Biodegrad 2012;73:23–32.
560   doi:10.1016/j.ibiod.2012.05.014.
561 [11] AWPA Standard. E24-06: Standard method of evaluating the resistance of evaluating the
562   resistance of wood product surfaces to mold growth. 2006.
563 [12] ASTM International. ASTM D3273-12: Standard Test Method for Resistance to Growth of Mold
564   on the Surface of Interior Coatings in an Environmental Chamber. 2012.
565 [13] British Standards Institute. BSI EN ISO 846: Plastics: Evaluation of the Action of
566   microorganisms. 1997.
567 [14] Amziane S, Collet F, Lawrence M, Magniont C, Picandet V, Sonebi M. Recommendation of the
568   RILEM TC 236-BBM: characterisation testing of hemp shiv to determine the initial water content,
569   water absorption, dry density, particle size distribution and thermal conductivity. Mater Struct
570   2017;50:167. doi:10.1617/s11527-017-1029-3.
571 [15] Rode C, Peuhkuri RH, Mortensen LH, Hansen KK, Time B, Gustavsen A, et al. Moisture
572   buffering of building materials. Technical University of Denmark, Department of Civil
573   Engineering; 2005.
574 [16] ISOBIO - Naturally High Performance Insulation 2015. http://isobioproject.com/.
575 [17] Collet F, Prétot S, Lanos C. Hemp-Straw Composites: Thermal And Hygric Performances.
576   Energy Procedia 2017;139:294–300. doi:10.1016/j.egypro.2017.11.211.

577 [18] Clausen CA, Yang VW. Image analysis for mould and sapstain detection on wood, Stockholm
578   (Sweden): 2013.
579 [19] Garzón-Barrero NM, Shirakawa MA, Brazolin S, de Barros Pereira RG de FN, de Lara IAR,
580   Savastano H. Evaluation of mold growth on sugarcane bagasse particleboards in natural
581   exposure and in accelerated test. Int Biodeterior Biodegrad 2016;115:266–76.
582   doi:10.1016/j.ibiod.2016.09.006.
583 [20] Blaber J, Antoniou A. Ncorr v1.2 n.d. http://www.ncorr.com/index.php/downloads (accessed
584   January 16, 2018).
585 [21] HOLO3, LMT-Cachan, Airbus Group Innovations. Correli STC. Correli STC n.d.
586   http://www.correli-stc.com/accueil.html (accessed January 16, 2018).
587 [22] Besnard G, Hild F, Roux S. "Finite-Element" Displacement Fields Analysis from Digital Images:
588   Application to Portevin–Le Châtelier Bands. Exp Mech 2006;46:789–803. doi:10.1007/s11340-
589   006-9824-8.
590 [23] Chu TC, Ranson WF, Sutton MA. Applications of digital-image-correlation techniques to
591   experimental mechanics. Exp Mech 1985;25:232–44. doi:10.1007/BF02325092.
592 [24] Sutton M, Orteu J-J, Schreier HW. Image Correlation for Shape, Motion and Deformation
593   Measurements. Basic Concepts, Theory and Applications. Springer US. 2009. doi:10.1007/978-
594   0-387-78747-3.
595 [25] Leveau J-Y, LARPENT J-P, BOUIX M. Sécurité microbiologique des procédés alimentaires.
596   Tech Ing Bioprocédés 2001.
597 [26] Heseltine E, Rosen J, World Health Organization, editors. Who guidelines for indoor air quality:
598   dampness and mould. Copenhagen: 2009.
599 [27] Stefanowski BK, Curling SF, Ormondroyd GA. A rapid screening method to determine the
600   susceptibility of bio-based construction and insulation products to mould growth. Int Biodeterior
601   Biodegrad 2017;116:124–32. doi:10.1016/j.ibiod.2016.10.025.
602 [28] Griffith GS, Boddy L. Fungal communities in attached ash (Fraxinus excelsior) twigs. Trans Br
603   Mycol Soc 1988;91:599–606. doi:10.1016/S0007-1536(88)80033-0.
604 [29] Li Y, Wadsö L. Fungal activities of indoor moulds on wood as a function of relative humidity
605   during desorption and adsorption processes. Eng Life Sci 2013;13:528–35.
606   doi:10.1002/elsc.201200100.
607 [30] Sharma PD. Ecology and environment. Rastogi Publications; 2012.
608 [31] Botton B, Breton A, Fevre M, Guy P, Larpent JP, Veau P. Moisissures utiles et nuisibles :
609   importance industrielle. Paris: Masson; 1985.
610 [32] Pitt JI, Hocking AD. Fungi and Food Spoilage. Springer Science & Business Media; 2009.
611 [33] Visagie CM, Houbraken J, Frisvad JC, Hong S-B, Klaassen CHW, Perrone G, et al. Identification
612   and nomenclature of the genus Penicillium. Stud Mycol 2014;78:343–71.
613   doi:10.1016/j.simyco.2014.09.001.
614 [34] Teófilo H, Ulloa M. El reino de los hongos: Micología básica y aplicada. Mexico: 2ª Edición
615   Fondo de Cultura Económica - UNAM; 1998.
616 [35] Thom C, Raper KB. The Aspergillus glaucus group. U.S. Dept. of Agriculture; 1941.
617 [36] Mitrović P, Marinković R. Phoma lingam–a rapeseed parasite in Serbia. Proc 12th Intern
618   Rapeseed Congr. Wuhan China, 2007, p. 217–219.
619 [37] Smith HC, Sutton BC. Leptosphaeria maculans the ascogenous state of Phoma lingam. Trans Br
620   Mycol Soc 1964;47:159-IN1. doi:10.1016/S0007-1536(64)80049-8.
621 [38] Travadon R. Facteurs épidémiologiques contribuant à l'adaptation des populations de
622   Leptosphaeria maculans aux résistances spécifiques de Brassica napus : dispersion des
623   pycnidiospores et des ascospores et progression systémique du champignon. phdthesis.
624   Agrocampus - Ecole nationale supérieure d'agronomie de rennes, 2008.
625

1   *Figure 1 : Flow-chart of composites production (except C4 formulation)*

2   *Figure 2 : Developed composites*

3   *Figure 3: Experimental device for biological aging: conditioning, weighing and photo recording*

4   *Figure 4: Digital image correlation between initial image f (time t_0) and current image g (time t)*

5   *Figure 5: Relative brightness, of image g and f: an error involves the detection of a new object.*

6   *Figure 6: Example of object detection using DIC*

7   *Figure 7: Procedure of image analysis, DIC and post-treatment applied on composite C5*

8   *Figure 8: Specimens on the weeks 0, 2, 4, 6, 8 and 12 of ageing test*

9   *Figure 9: Average rating of mold growth on specimens with the rating scale of BSI EN ISO 846 – 1997 (British*
10 *Standards Institute, 1997) after 12 weeks at 30°C and 90% RH*

11 *Figure 10: Variation of mass (at 30°C, 90% RH) from the steady state point at (23°C, 50% RH), related to the*
12 *exchange surface area*

13 *Figure 11: Mass loss for the tested composites during the ageing test*

14 *Figure 12 : Pictures before and after DIC treatment at the end of the test*

15 *Figure 13: Image analysis: rating of the contaminated surface of C2, C3, C4 and C5 composites exposed to 30°C*
16 *and 90% RH during the test period correlated to the fungal growth phases with I: Lag phase, II: Exponential*
17 *phase, III: Decelerating phase and IV: Stationary phase*

18 *Figure 14: Optical microscope visualizations contaminated surfaces at the 50x (a, b and c) and 125x (d and e)*
19 *magnifications (AR: Aspergillus ruber, ER: Eurotium rubrum, LM: Leptosphaeria maculans and PB: Penicillium*
20 *brevicompactum)*
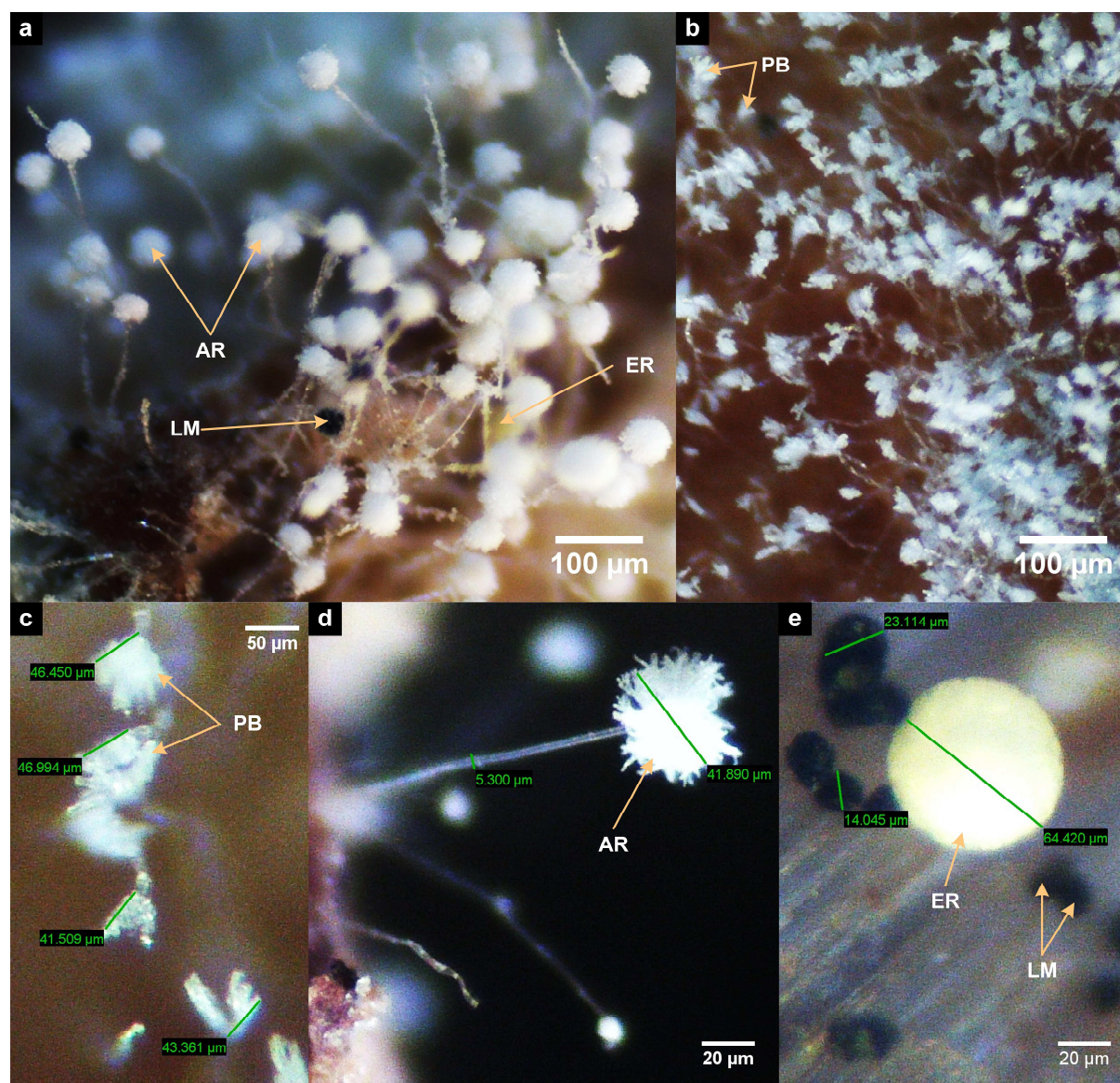
RESEARCH HIGHLIGHTS

- New rapid method for laboratory scale testing of materials resistance to molds.

- The fungal resistance of new bio-based buildings materials is analyzed.

- Mass monitoring overlaps the effect of water absorption and decay.

- DIC is used to analyze images. Correlation error indicates presence of mold.

- The pH of given building material is an important predictor of fungal susceptibility.